

This is the accepted manuscript made available via CHORUS, the article has been published as:

Kinematic cusps with two missing particles. II. Cascade decay topology

Tao Han, Ian-Woo Kim, and Jeonghyeon Song

Phys. Rev. D **87**, 035004 — Published 4 February 2013

DOI: [10.1103/PhysRevD.87.035004](https://doi.org/10.1103/PhysRevD.87.035004)

Kinematic Cusps with Two Missing Particles II: Cascade Decay Topology

Tao Han¹, Ian-Woo Kim², Jeonghyeon Song³

¹ *Pittsburgh Particle physics, Astrophysics, and Cosmology Center,
Department of Physics & Astronomy, University of Pittsburgh,
3941 O'Hara St., Pittsburgh, PA 15260, USA*

²*Department of Physics, University of Michigan, USA*

³*Division of Quantum Phases & Devices, School of Physics,
Konkuk University, Seoul 143-701, Korea*

Abstract

Three-step cascade decays into two invisible particles and two visible particles via two intermediate on-shell particles develop cusped peak structures in several kinematic distributions. We study their basic properties and demonstrate that the masses of the missing particles and the intermediate particles can be determined by the cusp and endpoint positions. Effects from realistic considerations such as finite decay widths, the longitudinal boost of the mother particle, the initial state radiation, and spin correlations are shown to be under control for the processes illustrated.

I. INTRODUCTION

At the energy frontier, the LHC experiments are taking us to an unprecedented territory of the Tera-scale physics beyond the Standard Model (SM). At the cosmo frontier, we have entered an era of precision cosmology. With much progress made in the two frontiers, we have to admit that our understanding of the universe is still far from being complete. According to the precise measurements of the cosmic microwave background fluctuations, such as WMAP [1], about 95% component of the current universe has never been directly observed in the laboratory. The dominant component ($\approx 72\%$) is dark energy that is responsible for the accelerating expansion of the universe [2]. The second dominant ($\approx 23\%$) is cold dark matter (CDM), which is assumed to be in a form of nonrelativistic matter but cannot be explained within the SM. Even in the realm of particle physics, the SM is regarded as an effective theory below a certain scale albeit its extraordinary success in explaining current experimental data with incredibly high precision. For example, theoretical unnaturalness of the SM, dubbed as the gauge hierarchy problem, suggests new physics beyond the SM at the TeV scale. Therefore, there is a very intriguing possibility that such CDM components appear in new particle physics models.

Indeed particle physics has theoretical answers for the astrophysical question about CDM. One of the most popular scenarios is a thermal production of weakly interacting massive particles [3]. In this scenario, a stable particle X had been once in thermal equilibrium in the early history of the universe, but later got frozen out as its reaction rate became slower than the expansion rate of the universe. The stability of the CDM particle over cosmic time is often attributed to an unbroken parity symmetry or a discrete symmetry. Under such a symmetry, the SM particle fields are in the trivial representation while new particle fields are in some nontrivial representation. The decay of the lightest new particle into SM particles is prohibited. The current observation highly suggests that the CDM particle has its mass at the electroweak scale and its couplings with a size of weak interaction. Some popular models with weakly interacting massive particles are supersymmetric models with R parity [4], the universal extra dimension (UED) model with Kaluza-Klein (KK) parity [5], and the littlest Higgs model with T parity [6].

This weakly interacting massive particle is likely to be produced at the LHC, and to be identified by missing transverse energy. The measurement of its mass is of crucial importance

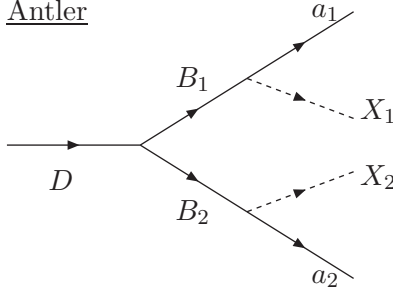


FIG. 1: The antler decay topology of a parity-even particle D into two missing particles (X_1 and X_2) and two visible particles (a_1 and a_2).

to reveal the identity of the CDM, but a very challenging task at the LHC because such invisible particles are produced in pairs. With large errors especially in jet energy measurements, the combinatoric complications disentangle the indirect information on the missing particle mass. In the literature, many new ideas to measure the CDM mass have been proposed [7], such as endpoint methods [8], polynomial methods [9, 10], M_{T2} methods [11–14], and combined methods [15].

Recently, we have proposed a new approach to measure the missing particle mass by using the singular structures in the kinematic distributions of the antler decay [16, 17]. The antler decay is a resonant decay of a parity-even particle D into a pair of the missing particles (X_1 and X_2) and a pair of SM visible particles (a_1 and a_2) through two on-shell parity-odd intermediate particles (B_1 and B_2), as depicted in Fig. 1. We have studied two kinds of singular structures, a cusp and an endpoint. The positions of cusps and endpoints determine the masses of the missing particle as well as the intermediate particle, if the mother particle mass m_D is known from other decay channels directly into two SM particles¹.

There are a few merits of this method: *(i)* the positions of the cusps and endpoints are stable under the spin correlation effects since it is purely determined by the phase space; *(ii)* a cusp as a sharp and non-smooth *peak* is statistically more advantageous to search than an endpoint, and more identifiable to observe than a kink; *(iii)* the simple configuration of outgoing particles can reduce combinatoric complication which is commonly troublesome in many missing particle mass measurement methods; *(iv)* the derived analytic functions of

¹ This is possible since the particle D has *even* parity.

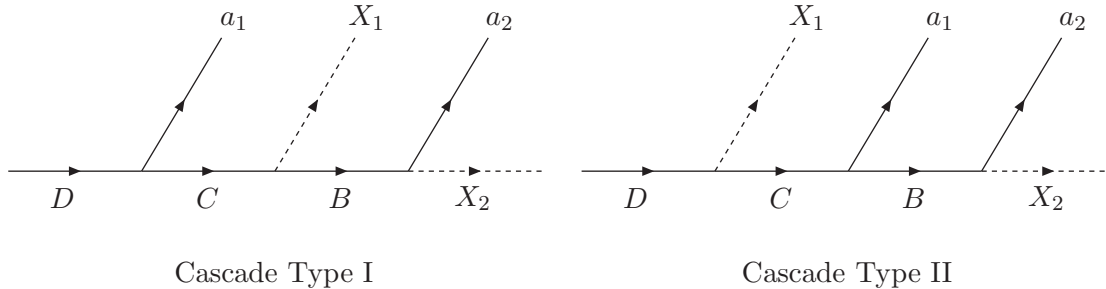


FIG. 2: The cascade decay topology of a parity-even particle D into two missing particles (X_1 and X_2) and two visible particles (a_1 and a_2).

some kinematic distributions allow us to reconstruct the mass parameters by best-fitting.

As a companion of Ref. [17], this paper focuses on another decay topology of a parity-even particle D into two visible particles and two missing particles, the *cascade* decay shown in Fig. 2. In this process, the mother particle D decays through three steps in series, finally ended up with a missing particle X_2 . There are two non-trivial types of this decay, TYPE I and TYPE II, according to at which step the first missing particle X_1 is produced. Unlike the antler decay case with one kind of intermediate particle, the cascade decay involves two different intermediate particles. We thus need to fix one more unknown mass, which requires more independent observables. The study of the basic properties of cusps and endpoints to determine all of the unknown masses is our main purpose. The cusp in the invariant mass distribution of the TYPE I cascade decay has been discussed in the context of new physics models with the CDM particle stabilized by Z_3 symmetry [18].

The rest of the paper is organized as follows. In Sec. II, we categorize all possible kinematic variables from the four-momenta of the two visible particles. Section III deals with the TYPE I cascade decay. We present the expressions of cusps and endpoints of various kinematic distributions in a common case where $m_{a_1} = m_{a_2} = 0$ and $m_{X_1} = m_{X_2}$. The functional form of the invariant mass distribution is also given. The general mass case is to be discussed in the Appendix. In Sec. IV, we present the corresponding results for the TYPE II cascade decay. Section V is devoted to realistic considerations such as the finite widths of the intermediate particles, the longitudinal boost of the mother particle D , the initial state radiation (ISR), and the spin correlation. We then conclude in Sec. VI.

II. KINEMATICS OF CASCADE DECAY TOPOLOGY WITH TWO MISSING PARTICLES

We consider the four-body cascade decay of a heavy particle D through three sequential steps. The cascade decay into a *single* missing particle and three visible particles has been extensively studied in the literature. In a supersymmetry model, a good example is the process of $\tilde{q} \rightarrow q\tilde{\chi}_2^0 \rightarrow q\ell_n\tilde{\ell} \rightarrow q\ell_n\ell_f\tilde{\chi}_1^0$. In the UED model, we have $Q^{(1)} \rightarrow Z^{(1)}q \rightarrow L^{(1)}\ell_nq \rightarrow B^{(1)}\ell_f\ell_nq$. Here $\ell_n(\ell_f)$ denotes the near (far) lepton with respect to the mother particle. In principle, three observable particles provide enough information to determine all of the unknown mass parameters [7, 8]. However, there are some difficulties in extracting proper information, especially because of combinatoric complications. It is hard to distinguish ℓ_n from ℓ_f . Furthermore, the mother particle D is to be pair-produced due to its odd parity, yielding another decay chain in the event.

Here we consider the three-step cascade decay with two missing particles. The mother particle D is of *even* parity and thus its single production is allowed. The final states are simply two visible particles (a_1 and a_2) with missing transverse energy. There is no combinatoric complication when forming the invariant mass of two visible particles. In addition, if the rest frame of D in the transverse direction can be determined, we can use the transverse momenta of a_1 and a_2 as additional information. As shall be shown below, some transverse momentum variable distributions accommodate cusps.

The cascade decays of $D \rightarrow a_1a_2X_1X_2$ can be classified according to at which step the first missing particle, say X_1 , is produced. We fix that the other missing particle X_2 is from the last step. If X_1 is also from the last step, the final intermediate particle B is just missing and this decay is indistinguishable from a two step cascade decay. We do not consider this case. Then, there are two non-trivial three-step cascade decays, as depicted in Fig. 2. In the TYPE I decay, X_1 is from the second step. The mother particle D decays into a visible particle a_1 and a new particle C , followed by the decay of C into a missing particle X_1 and a new particle B . Finally B decays into a visible particle a_2 and a missing particle X_2 . In the TYPE II decay, X_1 is from the first step: D decays into CX_1 , followed by $C \rightarrow a_1B$, and finally $B \rightarrow a_2X_2$. In the view point of two observable particles a_1 and a_2 , this TYPE II decay is a two-step cascade decay of a new heavy particle C . As shall be shown, there is no cusp structure in Lorentz-invariant distributions.

It is useful to describe the kinematics in terms of the rapidity of a massive particle i :

$$\eta_i^{(k)} = \frac{E_i^{(k)}}{m_i}, \quad (1)$$

where $E_i^{(k)}$ and m_i are the energy and mass of the particle i in the rest frame of a particle (system) k . To avoid confusion, we adopt the following rapidity notations for the TYPE I and TYPE II decays:

	TYPE I Cascade	TYPE II Cascade
rapidity notation	ξ_i	ζ_i

(2)

For the sake of simplicity, we omit the superscript specifying the reference frame when the rapidity is defined in the rest frame of its mother particle.

With the four-momenta k_1 and k_2 of the two observable particles a_1 and a_2 in the lab frame, respectively, we consider the following observables in three categories:

- Lorentz invariant observables: the invariant mass of a_1 and a_2 ,

$$m = \sqrt{(k_1 + k_2)^2}. \quad (3)$$

- Longitudinal-boost invariant observables:

- the magnitude of the transverse momentum of a visible particle a_i ,

$$p_{Ti} = |\mathbf{k}_i^T|, \quad (4)$$

- the magnitude of the transverse momentum of the a_1 - a_2 system,

$$p_T = |\mathbf{k}_1^T + \mathbf{k}_2^T|, \quad (5)$$

- the transverse mass of the a_1 - a_2 system,

$$m_T = \sqrt{p_T^2 + m^2}. \quad (6)$$

- Non-invariant observables:

- cosine of Θ_i , the angle of the visible particle a_i in the c.m. frame of a_1 and a_2 , with respect to their c.m. moving direction,

$$\cos \Theta = \frac{\mathbf{k}_1^{(aa)} \cdot \mathbf{k}^{(D)}}{|\mathbf{k}_1^{(aa)}| |\mathbf{k}^{(D)}|}. \quad (7)$$

Here the bold-faced letter denotes the three-vector momentum, $k = k_1 + k_2$, and the superscript (D) and (aa) denote the D -rest frame and the c.m. frame of a_1 and a_2 , respectively. We note that the $\cos \Theta$ variable is observable only if the rest frame of the mother particle D is reconstructed.

As shall be shown, p_{Ti} and m_T distributions show cusp structures if the mother particle D is produced at rest in the transverse direction. These additional cusp structures are very valuable to determine all of the unknown masses. At a hadron collider, however, reconstructing the transversely rest frame of D is not feasible since strong QCD interactions always yield sizable ISR, which causes transverse kick to the mother particle D . The cusps and endpoints in the D rest frame get affected. In Sec. V, we study the ISR effects on the m_T and p_{Ti} cusps and endpoints.

The final comment in this section is on the simplifying assumption about mass parameters. In general, the involved seven particles ($D, C, B, a_1, a_2, X_1, X_2$) may have different masses. However, the cascade decay processes in many new physics models have massless visible particles and the same kind of invisible particles. In the main text, therefore, we consider only the following case:

$$m_{a_1} = m_{a_2} = 0, \quad m_{X_1} = m_{X_2}. \quad (8)$$

The results for the most general case with seven different masses are presented in the Appendix.

III. TYPE I CASCADE DECAY

As illustrated in Fig. 2, the TYPE I cascade decay is the decay of a parity-even particle D into two missing particles X_1 and X_2 and two visible particles a_1 and a_2 through

$$\begin{aligned} D(P) &\longrightarrow C + a_1(k_1), \\ C &\longrightarrow B + X_1, \\ B &\longrightarrow a_2(k_2) + X_2. \end{aligned} \quad (9)$$

Here D, C, a_1 , and a_2 are parity-even while B, X_1 , and X_2 are parity-odd. In order to accommodate the TYPE I cascade decay, we need at least two heavy parity-even particles.

One good example is found in the UED model [19]. It is based on a single flat extra dimension of size R , compactified on an S_1/Z_2 orbifold. All of the SM fields propagate

	m_D	m_C	m_B	m_X	ξ_B
MASS-A ₁	1045.7	1023.	514.2	500.9	0.12
MASS-B ₁	600	400	200	100	0.60
MASS-C ₁	600	500	150	100	1.16

TABLE I: Test mass spectrum sets for the TYPE I cascade decay. All of the masses are in units of GeV.

freely in the whole five-dimensional spacetime. Each field has an infinite number of KK excited states. Since the KK parity is conserved, the lightest KK particle with odd KK parity is stable and becomes a good candidate for the CDM. Usually the first KK mode of the $U(1)_Y$ gauge boson $B^{(1)}$ is the lightest KK particle [19, 20]. All of the second KK states of the SM particles have even KK-parity and mass of $\sim 2/R$. Lower limit of $1/R \gtrsim 400$ GeV is set based on the combination of the constraints from the ρ parameter [21], the electroweak precision tests [22], the muon $g - 2$ measurement [23], the flavor changing neutral currents [24], the direct searches by the D0 collaborations at the Tevatron [25] and the ATLAS and CMS collaborations [26]. The second KK modes are within the reach of the LHC. Possible TYPE I cascade decays are

$$Z^{(2)} \rightarrow \ell_n + L^{(2)} \rightarrow \ell_n + B^{(1)} L^{(1)} \rightarrow \ell_n + B^{(1)} + \ell_f B^{(1)}, \quad (10)$$

$$g^{(2)} \rightarrow q_n + q^{(2)} \rightarrow q_n + B^{(1)} q^{(1)} \rightarrow q_n + B^{(1)} + q_f B^{(1)}. \quad (11)$$

Now we present the cusps and endpoints of m , m_T , p_T , p_{Ti} , and $\cos \Theta$ distributions in terms of the masses. For the simple case in Eq. (8), there are two independent rapidities, ξ_B and ξ_C , given by

$$\cosh \xi_B = \frac{m_C}{2m_B} \left(1 + \frac{m_B^2}{m_C^2} - \frac{m_X^2}{m_C^2} \right), \quad \cosh \xi_C = \frac{m_D}{2m_C} \left(1 + \frac{m_C^2}{m_D^2} \right). \quad (12)$$

We will also use E_n and E_f , the energy of the near visible particle a_1 and the far visible particle a_2 in its mother's rest frame, respectively:

$$E_n = \frac{m_D}{2} \left(1 - \frac{m_C^2}{m_D^2} \right), \quad E_f = \frac{m_B}{2} \left(1 - \frac{m_X^2}{m_B^2} \right). \quad (13)$$

For illustration, we take three sets for the mass parameters in Table I. The MASS-A₁ is motivated by the $Z^{(2)}$ decay in Eq. (10). The KK masses are determined by the UED model parameters of $\Lambda R = 20$ and $1/R = 500$ GeV, where Λ is the cutoff scale [19]. Almost

equal spacing in the KK mass spectrum leads to very degenerate masses, *i.e.*, $m_D \approx m_C \approx 2m_B \approx 2m_X$. The MASS-B₁ case has substantial mass gaps for each pair of adjacent masses. Finally the MASS-C₁ case has a sizable mass gap between m_C and $m_B + m_X$.

For the precise mass measurement using the singularities, it is necessary to have visible cusp and endpoint. A sharp cusp is considered as a visible one. The visibility of an endpoint is determined by the functional behavior near the endpoint, either fast dropping or long-tailed. We take the former as a visible endpoint.

(i) Invariant mass m distribution: We first discuss the distribution of the invariant mass m of two visible particles. The differential decay rate $d\Gamma/dm$ is

$$\frac{d\Gamma}{dm} \propto \begin{cases} 2\xi_B m, & \text{for } 0 < m < m_{\text{cas1}}^{\text{cusp}}, \\ m \ln \frac{(m_{\text{cas1}}^{\text{max}})^2}{m^2}, & \text{for } m_{\text{cas1}}^{\text{cusp}} < m < m_{\text{cas1}}^{\text{max}}, \end{cases} \quad (14)$$

where the cusp and endpoint are

$$(m_{\text{cas1}}^{\text{cusp}})^2 = 4E_n E_f e^{\xi_C - \xi_B}, \quad (m_{\text{cas1}}^{\text{max}})^2 = 4E_n E_f e^{\xi_C + \xi_B}. \quad (15)$$

Note that the functional behavior of $d\Gamma/dm$ is the same as that of the antler decay [17]. The general case with 7 different masses is discussed in the Appendix.

The degree of the sharpness of the m cusp is deduced from Eq. (14). The $d\Gamma/dm$ function is linear in m for $m < m_{\text{cas1}}^{\text{cusp}}$, and a concave function for $m_{\text{cas1}}^{\text{cusp}} < m < m_{\text{cas1}}^{\text{max}}$. At $m = m_{\text{cas1}}^{\text{max}}/e$, the concave function reaches its maximum. If $m_{\text{cas1}}^{\text{max}}/e < m_{\text{cas1}}^{\text{cusp}}$, which is equivalent to $\xi_B < 1$, the cusp can be considered to be pronounced.

In Fig. 3, we show the normalized differential decay rate $d\Gamma/dm$ for the three mass parameter sets in Table I. In order to compare the shapes of cusps only, we present it as a function of $m/m_{\text{cas1}}^{\text{max}}$. The vertical lines denote the positions of $m_{\text{cas1}}^{\text{cusp}}$ in units of $m_{\text{cas1}}^{\text{max}}$. The MASS-A₁ case with $\xi_B = 0.12$ has a very sharp m cusp. The MASS-B₁ case with $\xi_B = 0.60$ shows a triangular shape with a cusped peak. However, the MASS-C₁ case with $\xi_B = 1.16$ has a dull cusp. The endpoints for all of three cases are fast dropping, as suggested by the concave function in Eq. (14).

(ii) Transverse mass m_T distribution: Figure 4 shows the normalized differential decay rate $d\Gamma/dm_T$, which is defined in the rest frame of D . For all of three cases, the m_T distributions show visible cusp structures. Even the MASS-C₁ case, which has a dull cusp in the m distribution, has a quite sharp cusp. This is contrasted to the antler decay case where

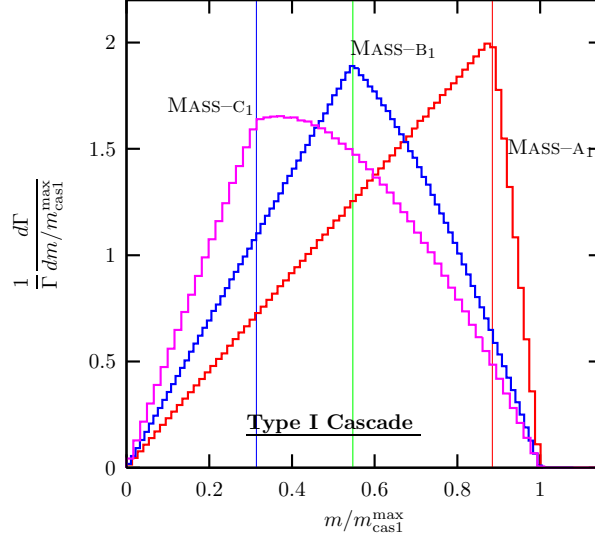


FIG. 3: The normalized differential decay rate of the invariant mass of two visible particles, $\frac{d\Gamma}{\Gamma dm}$ for the TYPE I cascade decay. The masses are in Table I.

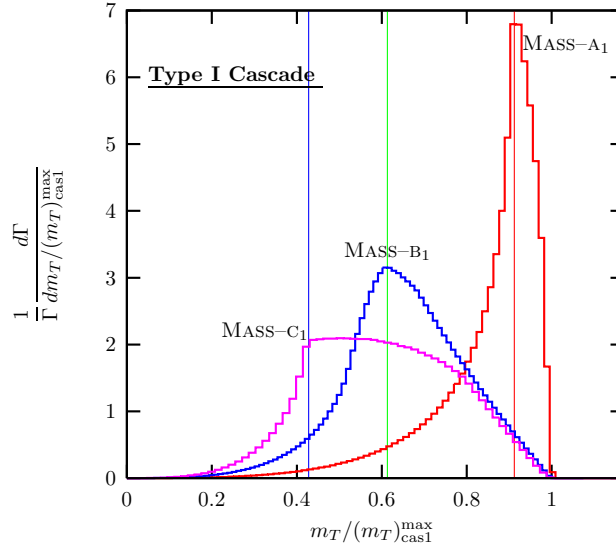


FIG. 4: The normalized differential decay rate of the transverse mass of two visible particles, $\frac{d\Gamma}{\Gamma dm_T}$ for the TYPE I cascade decay. The masses are in Table I.

there is no cusp in the m_T distribution [17]. As shall be shown in the next section, the TYPE II cascade decay also has a cusp in the m_T distribution. Therefore the presence of the m_T cusp signals the cascade decay topology. The cusp and maximum positions in terms of the masses are

$$(m_T)_{\text{cas1}}^{\text{cusp}} = E_n + E_f e^{\xi_C - \xi_B}, \quad (m_T)_{\text{cas1}}^{\text{max}} = E_n + E_f e^{\xi_C + \xi_B}, \quad (16)$$

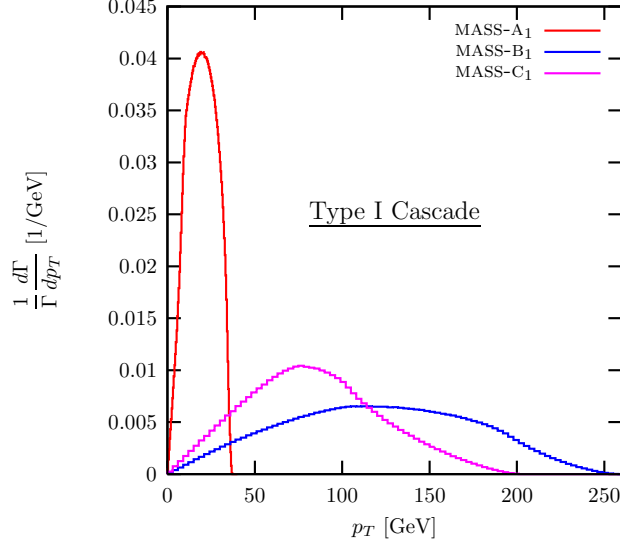


FIG. 5: The normalized differential decay rate of the transverse momentum of two visible particles, $\frac{d\Gamma}{\Gamma dp_T}$ for the TYPE I cascade decay for the masses in Table I.

where E_n and E_f are in Eq. (13).

(iii) The system p_T distribution: Figure 5 shows the normalized distribution of the transverse momentum p_T of two visible particle system. For all of the three mass spectra in Table I, the p_T distribution has smooth peak without a cusp structure. The endpoint of p_T distribution is

$$(p_T)_{\text{cas1}}^{\text{max}} = E_n + E_f e^{-\xi_C + \xi_B}. \quad (17)$$

Only the MASS-A₁ case has the endpoint of fast-dropping shape, which is attributed to very small momentum transfer to the visible particles. More general cases of MASS-B₁ and MASS-C₁ have long-tailed endpoints. The p_T distribution is not useful for the mass measurement.

(iv) Single particle p_{Ti} distribution: We show the individual transverse momentum p_{Ti} distributions in Fig. 6. The thin solid line labeled by “near” (“far”) is the p_{Ti} distribution of the near visible particle a_1 (the far visible particle a_2). The p_{Tf} distribution has both the cusp and the endpoint structures. On the contrary, the p_{Tn} distribution has only an endpoint of a suddenly ending shape, which holds true for all of the mass cases. The positions of the cusp and the endpoint in the p_{Tf} distribution are given by

$$(p_{Tf})_{\text{cas1}}^{\text{cusp}} = E_f e^{\xi_C - \xi_B}, \quad (p_{Tf})_{\text{cas1}}^{\text{max}} = E_f e^{\xi_C + \xi_B}, \quad (18)$$

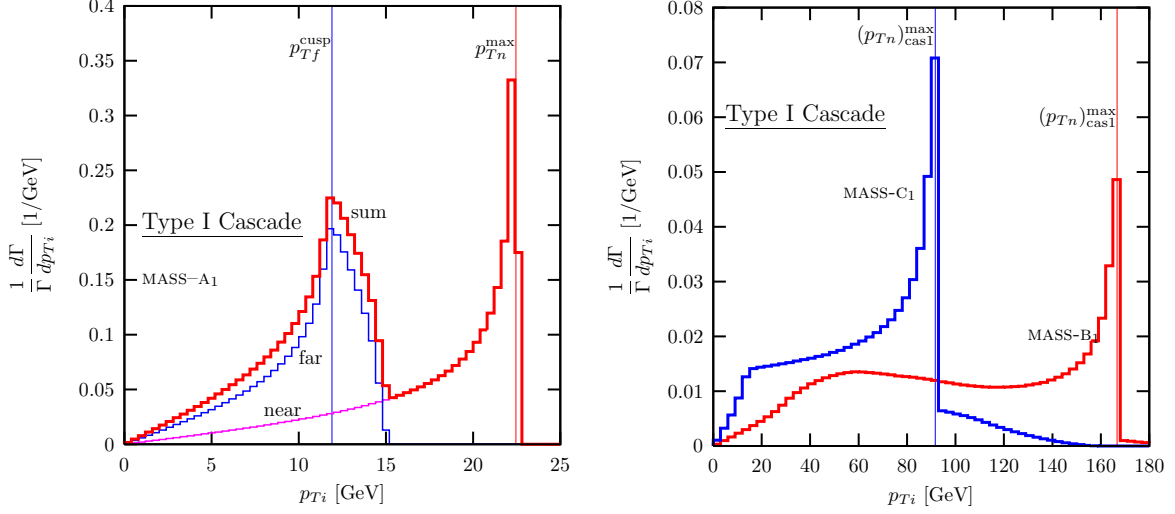


FIG. 6: The normalized differential decay rate of the transverse momentum of one visible particle, $\frac{d\Gamma}{\Gamma dp_{Ti}}$ for the TYPE I cascade decay. In the MASS-A₁ case, the line labeled by “near” (“far”) denotes the p_{Ti} distribution of a_1 (a_2). Thick lines are the summed distributions of p_{Ti} .

and the endpoint in the p_{Tn} distribution is located at

$$(p_{Tn})_{cas1}^{max} = E_n. \quad (19)$$

However, we cannot distinguish a_1 from a_2 event by event. Therefore we consider a more practical observable, the sum of two p_{Ti} distributions. The thick lines in Fig. 6 represent the sum. Depending on whether $(p_{Tn})_{cas1}^{max} > (p_{Tf})_{cas1}^{max}$ or not, the summed distribution shows very different shape. For the former case as in MASS-A₁, the spiky $(p_{Tn})_{cas1}^{max}$ stands outside the p_{Tf} distribution, which reveals the p_{Tf} cusp and endpoint. For the later case as in MASS-B₁ and MASS-C₁, the $(p_{Tn})_{cas1}^{max}$ peak lies in the middle of p_{Tf} distribution. The p_{Tf} cusp gets distorted and thus barely visible.

(v) $\cos \Theta$ distribution: The variable $\cos \Theta$ in Eq. (7) is defined by the angle of *one* visible particle. We have two $\cos \Theta$ distributions for a_1 and a_2 , which cannot be distinguished. In Fig. 7, therefore, we present the summation of two $\cos \Theta_i$ distributions in the rest frame of D for MASS-A₁ and MASS-B₁ cases. It is symmetric about $\cos \Theta = 0$, and has two cusp structures, $\cos \Theta_{cas1}^{cusp1}$ and $\cos \Theta_{cas1}^{cusp2}$, marked by the vertical arrows. In terms of masses, they are

$$\cos \Theta_{cas1}^{cusp1} = \frac{E_n - E_f \exp(\xi_B - \xi_C)}{E_n + E_f \exp(\xi_B - \xi_C)}, \quad \cos \Theta_{cas1}^{cusp2} = \frac{E_n - E_f \exp(-\xi_B - \xi_C)}{E_n + E_f \exp(-\xi_B - \xi_C)}. \quad (20)$$

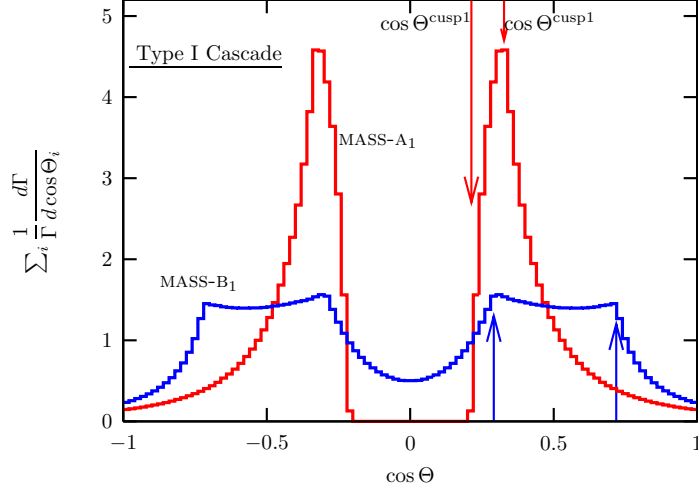


FIG. 7: The summed distributions of $\cos \Theta_i$ in the TYPE I cascade decay for the masses in Table I.

In the MASS- A_1 case, $\cos \Theta_{\text{cas}1}^{\text{cusp}1}$ stands on a steep slope, which is difficult to probe. The MASS- B_1 case shows two pronounced cusps.

IV. TYPE II CASCADE DECAY

TYPE II cascade decay is a chain decay of

$$\begin{aligned} D(P) &\longrightarrow C + X_1, \\ C &\longrightarrow B + a_1(k_1), \\ B &\longrightarrow a_2(k_2) + X_2. \end{aligned} \tag{21}$$

A good example can be found in the MSSM:

$$H/A \rightarrow \tilde{\chi}_1^0 + \tilde{\chi}_2^0, \quad \tilde{\chi}_2^0 \rightarrow \ell_n + \tilde{\ell}, \quad \tilde{\ell} \rightarrow \ell_f + \tilde{\chi}_1^0. \tag{22}$$

As in the TYPE I cascade decay, we restrict ourselves to the realistic cascade decay with $m_{a_1} = m_{a_2} = 0$ and $m_{X_1} = m_{X_2}$. Then there are two independent rapidities, ζ_C and ζ_B :

$$\cosh \zeta_B = \frac{m_C}{2m_B} \left(1 + \frac{m_B^2}{m_C^2} \right), \quad \cosh \zeta_C = \frac{m_D}{2m_C} \left(1 + \frac{m_C^2}{m_D^2} - \frac{m_X^2}{m_D^2} \right). \tag{23}$$

For illustration, we consider three mass sets for the TYPE II cascade decay in Table II.

(i) Invariant mass m distribution: We first study the distribution of the invariant mass of a_1 and a_2 . Note that in the view point of a_1 and a_2 , this TYPE II cascade decay is a three

	m_D	m_C	m_B	m_X	m^{\max}
MASS-A ₂	614	299	222	161	138.0
MASS-B ₂	600	300	200	100	193.6
MASS-C ₂	400	250	150	120	120.0

TABLE II: Test mass spectrum sets for the TYPE II cascade decay. All of the masses are in units of GeV.

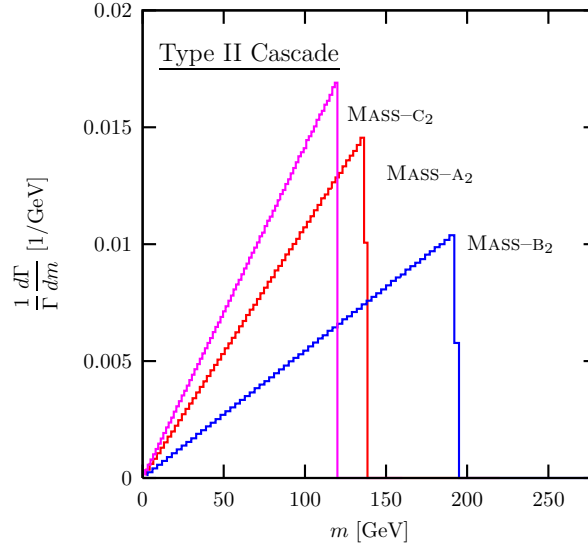


FIG. 8: The normalized differential decay rate of the invariant mass of two visible particles, $\frac{d\Gamma}{\Gamma dm}$ for the TYPE II cascade decay. The mass spectrum sets are described in Table II.

body decay of the mother particle C . The presence of the invisible X_1 decayed from D does not change any Lorentz invariant result. The m distribution is the same as that of, *i.e.*, $m_{\ell\ell}$ of the decay $\tilde{\chi}_2^0 \rightarrow \ell_n \tilde{\ell} \rightarrow \ell_n \ell_f \tilde{\chi}_1^0$ in the MSSM. This $m_{\ell\ell}$ distribution is well known to have no cusp structure. The endpoint is [27]

$$(m_{\text{cas2}}^{\max})^2 = m_C^2 \left(1 - \frac{m_B^2}{m_C^2}\right) \left(1 - \frac{m_X^2}{m_B^2}\right). \quad (24)$$

In Fig. 8, we show the m distribution for three sets of the mass parameters in Table II, all of which have right-angled triangle shapes without a cusp.

The absence of a cusp in a two-step cascade decay can be understood by a simple kinematic configuration. For the antler decay ($D \rightarrow B_1 + B_2 \rightarrow a_1 X_1 + a_2 X_2$) in the massless visible particle case ($m_{a_1} = m_{a_2} = 0$), the following four critical points correspond to a

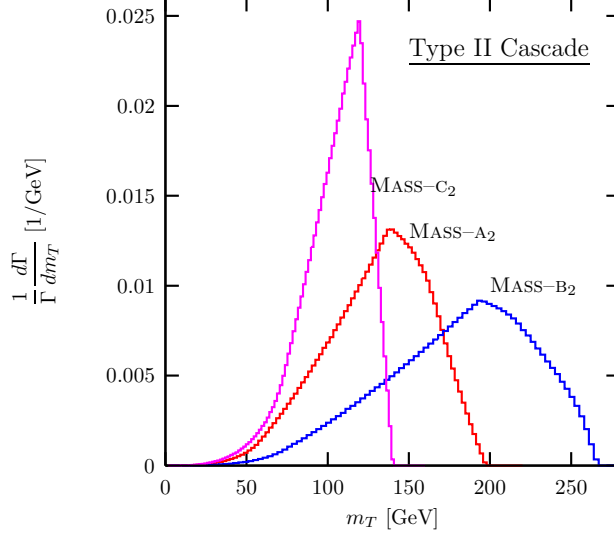


FIG. 9: The normalized differential decay rate of the transverse mass of two visible particles, $\frac{d\Gamma}{dm_T}$ for the TYPE II cascade decay. The mass spectrum sets are described in Table II.

kinematic singular structure [17]:

1D configuration					$m_{a_1 a_2}$
$\overleftarrow{a_2}$	$\overleftarrow{B_2}$	$\begin{matrix} D \\ \bullet \end{matrix}$	$\overrightarrow{B_1}$	$\overrightarrow{a_1}$	max
$\overrightarrow{a_2}$	$\overleftarrow{B_2}$	\bullet	$\overrightarrow{B_1}$	$\overleftarrow{a_1}$	cusp
$\overrightarrow{a_2}$	$\overleftarrow{B_2}$	\bullet	$\overrightarrow{B_1}$	$\overrightarrow{a_1}$	min
$\overleftarrow{a_2}$	$\overleftarrow{B_2}$	\bullet	$\overrightarrow{B_1}$	$\overleftarrow{a_1}$	min

(25)

Here we simplify the picture as an one-dimensional case. It is clear to see that $m_{a_1 a_2}^{\min}$ happens when two observable particles move in the same direction, while one of two kinematic configurations of back-to-back moving visible particles corresponds to either $m_{a_1 a_2}^{\max}$ or $m_{a_1 a_2}^{\text{cusp}}$. For a two-step cascade decay ($C \rightarrow a_1 + B \rightarrow a_1 + a_2 X_2$), a_1 and a_2 in one-dimensional space have only two independent kinematic configurations, moving in the same direction and moving in the opposite direction. The former corresponds to the minimum m , while the later to the maximum m . There is no critical point left for the cusp.

(ii) Transverse mass m_T distribution: Unlike the invariant mass distribution, the m_T distribution contains the information about the transverse momentum of the first missing particle X_1 . As shown in Fig. 9, there is a cusp here. We stress once again that this m_T cusp appears only when D is produced at rest in the transverse direction.

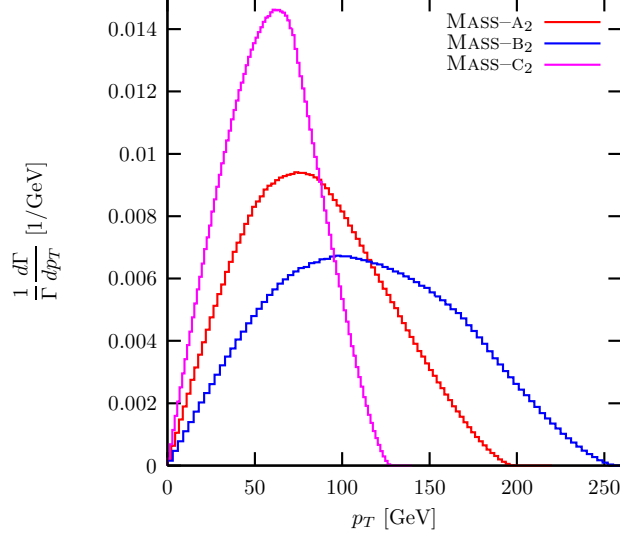


FIG. 10: The normalized differential decay rate of the transverse momentum of two visible particles, $\frac{d\Gamma}{\Gamma dp_T}$ for the TYPE II cascade decay. The mass spectrum sets are in Table II.

Another interesting feature is that the position of the m_T cusp is nothing but the m maximum:

$$(m_T)_{\text{cas2}}^{\text{cusp}} = m_{\text{cas2}}^{\text{max}}. \quad (26)$$

This non-trivial equality is a unique feature of the TYPE II cascade decay.

(iii) System p_T distribution: The total p_T distributions for the TYPE II cascade decay are shown in Fig. 10. All of the three mass sets have smooth p_T distributions. And their endpoints are all long-tailed. This feature is common for the antler, TYPE I, and TYPE II cascade decay topology.

(iv) Single particle p_{Ti} distribution: Figure 11 shows the distribution of the individual transverse momentum of the near a_1 and the far a_2 . The near p_{Tn} distribution has a sharp cusp and a fast dropping endpoint. The p_{Tf} distribution has a long tailed endpoint without any cusp. In terms of masses they are simply

$$(p_{Tn})_{\text{cas2}}^{\text{cusp}} = \frac{m_C}{2} \left(1 - \frac{m_B^2}{m_C^2} \right) e^{-\zeta_C}, \quad (p_{Tn})_{\text{cas2}}^{\text{max}} = \frac{m_C}{2} \left(1 - \frac{m_B^2}{m_C^2} \right) e^{\zeta_C}. \quad (27)$$

Note that the product of $(p_{Tn})_{\text{cas2}}^{\text{cusp}}$ and $(p_{Tn})_{\text{cas2}}^{\text{max}}$ removes the ζ_C dependence, which depends on the intermediate masses m_C and m_B . In addition the ratio $(p_{Tn})_{\text{cas2}}^{\text{cusp}}/(p_{Tn})_{\text{cas2}}^{\text{max}}$ depends only on the rapidity ζ_C .

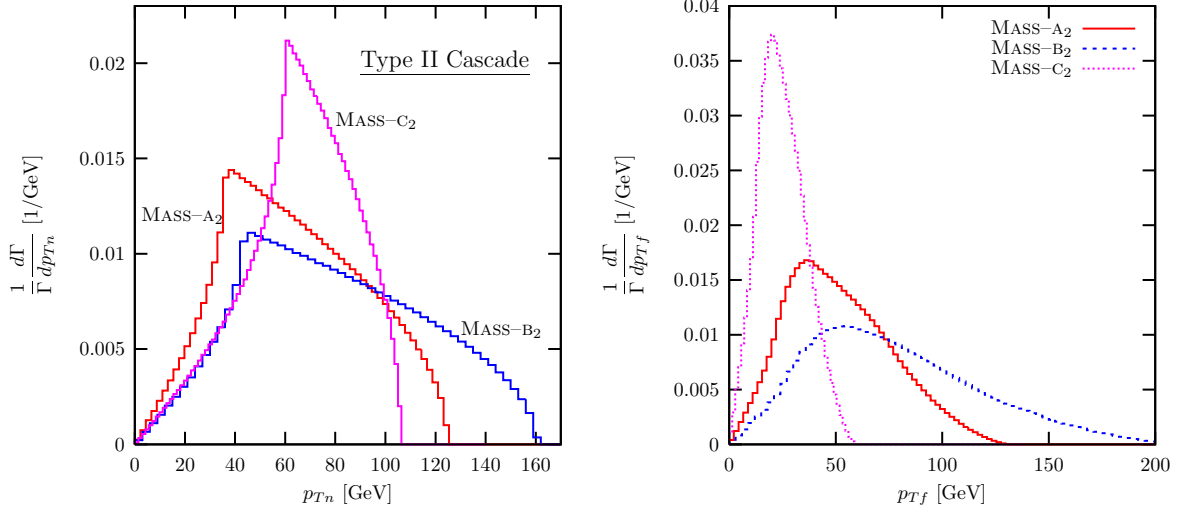


FIG. 11: The normalized differential decay rate of the transverse mass of one visible particle, $\frac{d\Gamma}{\Gamma dp_{Ti}}$ for the TYPE II cascade decay. The left figure is for the near visible particle a_1 , and the right one is for the far visible particle a_2 .

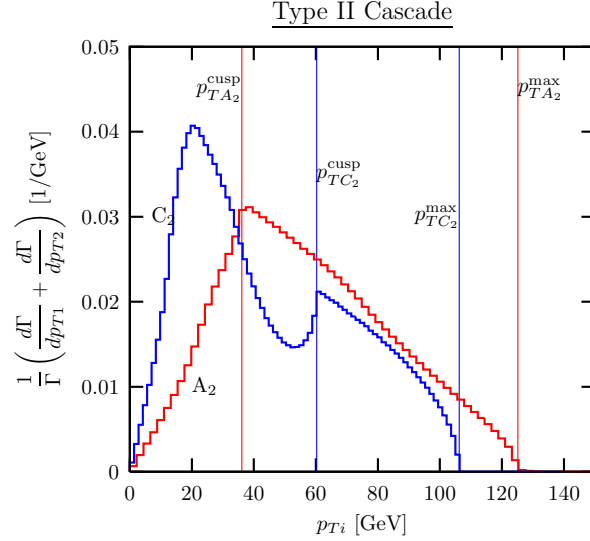


FIG. 12: The sum of two normalized differential decay rate with respect to the individual transverse momenta of the near and far visible particles.

As discussed before, the individual p_{Ti} distribution cannot be constructed. Instead we show the sum of two distributions in Fig. 12. For the MASS- A_2 case, the cusp in the p_{Tn} distribution and the smooth peak of the p_{Tf} distribution are located nearby. In their sum, the p_{Tn} cusp survives over the relatively round p_{Tf} peak and the fast dropping p_{Tn} endpoint is also measurable. For the MASS- C_2 case, however, the p_{Tn} cusp and the p_{Tf} peak are

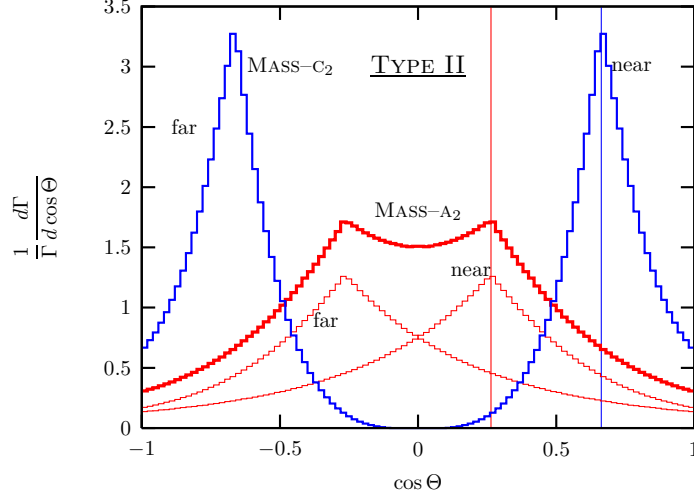


FIG. 13: The sum of $d\Gamma/d\cos\Theta_i$ for the TYPE II cascade decay.

separated so that the summed distribution shows both. With finite number of data, it would be difficult to distinguish the p_{Tn} cusp from the p_{Tf} peak.

(v) The $\cos\Theta$ distribution: We consider the $\cos\Theta$ distribution for the TYPE II cascade decay. In Fig. 13 we show the normalized differential decay rate $d\Gamma/d\cos\Theta$ for the near and far visible particles (denoted by thin lines) as well as their sum (thick lines) for the MASS-A₂ and MASS-C₂. In both cases, the summed distribution of $\cos\Theta_i$ is symmetric about $\cos\Theta = 0$, and has one sharp cusp denoted by vertical lines in Fig. 13. The $\cos\Theta$ cusp position in terms of the mass parameters is

$$\cos\Theta_{\text{cas2}}^{\text{cusp}} = \frac{m_C \left(1 - \frac{m_B^2}{m_C^2}\right) - m_B \left(1 - \frac{m_X^2}{m_B^2}\right) e^{-\zeta_B}}{m_C \left(1 - \frac{m_B^2}{m_C^2}\right) + m_B \left(1 - \frac{m_X^2}{m_B^2}\right) e^{-\zeta_B}}. \quad (28)$$

(vi) Mass determination from the cusps and endpoints: Unlike the antler decay with one kind of intermediate particles, the cascade decay has two different intermediate particles. In addition, the TYPE II decay has fewer independent observables of cusps and endpoints: there is no m cusp structure; the m_T cusp position is the same as the m endpoint. A concern arises whether we have enough information to determine all of the masses, especially at the LHC where the $\cos\Theta$ cusp cannot be used. We show that three unknown masses (m_C , m_B , and m_X) are unambiguously determined by three singularities of $m_{\text{cas2}}^{\text{max}}$, $(p_{Tn})_{\text{cas2}}^{\text{cusp}}$, and $(p_{Tn})_{\text{cas2}}^{\text{max}}$, as

$$m_C = R_\alpha m_D, \quad m_B = \sqrt{1 - \frac{\alpha_1}{R_\alpha}} m_C, \quad m_X = \sqrt{1 - \frac{\alpha_2}{R_\alpha}} m_B, \quad (29)$$

where R_α is

$$R_\alpha = \frac{1 + \alpha_1 \alpha_2}{\alpha_3 - \alpha_1 - \alpha_2}, \quad (30)$$

and $\alpha_{1,2,3}$ are

$$\begin{aligned} \alpha_1 &= \frac{(m_{\text{cas}2}^{\text{max}})^2}{2m_D \sqrt{(p_{Tn})_{\text{cas}2}^{\text{max}} / (p_{Tn})_{\text{cas}2}^{\text{cusp}}}}, \\ \alpha_2 &= \frac{2\sqrt{(p_{Tn})_{\text{cas}2}^{\text{max}} / (p_{Tn})_{\text{cas}2}^{\text{cusp}}}}{m_D}, \\ \alpha_3 &= \sqrt{\frac{(p_{Tn})_{\text{cas}2}^{\text{max}}}{(p_{Tn})_{\text{cas}2}^{\text{cusp}}}} + \sqrt{\frac{(p_{Tn})_{\text{cas}2}^{\text{cusp}}}{(p_{Tn})_{\text{cas}2}^{\text{max}}}}. \end{aligned} \quad (31)$$

V. EFFECTS OF REALISTIC CONSIDERATIONS

All of the previous expressions of the cusps and endpoints have been derived in an idealistic situation: the total decay widths of decaying particles are ignored; the D rest frame is assumed to be reconstructed; the ISR effects are neglected; the spin-correlation effects from the full matrix elements are negligible. In this section, we investigate these effects on the position and shape of the kinematic cusp and endpoint.

A. Finite width effects

Up to now we have applied the narrow width approximation, ignoring the width of decaying particles. Since the effect of finite Γ_D is shown to be very minor in Ref. [16], we focus on the effects of Γ_B and Γ_C .

We find that the mass spectrum is the most crucial factor to determine the stability of the cusp and endpoint structures under the width effects. Out of six cases in Tables I and II, the MASS-A₁ has very vulnerable structures. This case is special because of its degenerate masses: the observable particles have very small momentum transfer and their kinematic phase space is highly limited.

In Fig. 14 and Fig. 15, we show, for the MASS-A₁ case, the finite width effects on the m , m_T , $\sum p_{Ti}$, and $\cos \Theta$ distributions. We present four cases for Γ_B and Γ_C : on-shell (solid line), $\Gamma/M = 0.01$ (long dashed line), $\Gamma/M = 0.1$ (short dashed line), and $\Gamma/M = 0.5$ (dotted line). Here $\Gamma/M \equiv \Gamma_B/m_B = \Gamma_C/m_C$ for simplicity. Just one percent of Γ/M

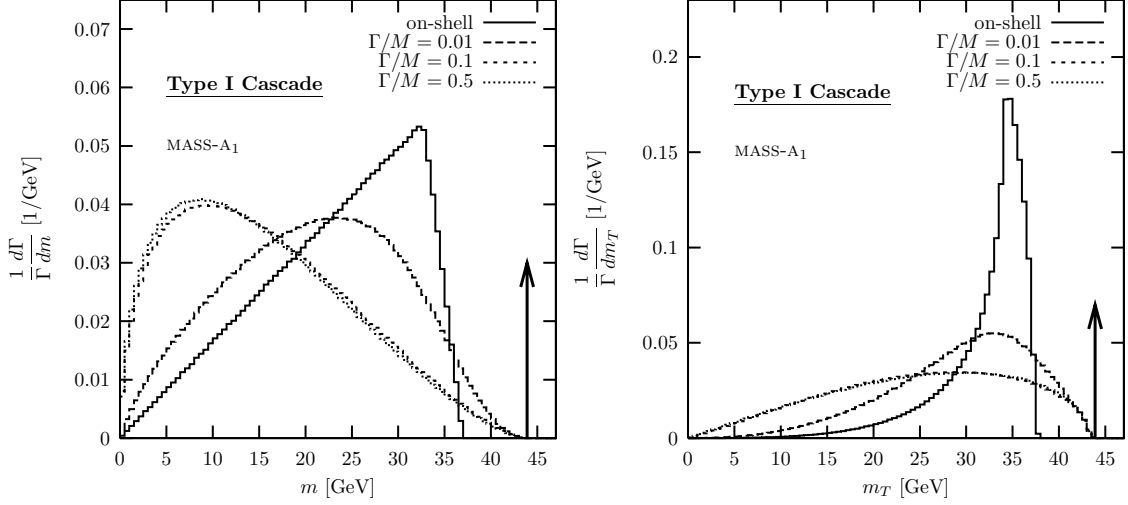


FIG. 14: The finite decay width effects on the m and m_T distributions in the MASS-A₁ case. Solid lines are for the on-shell decay, the long dashed lines for $\Gamma/M = 0.01$, the short dashed lines for $\Gamma/M = 0.1$, and the dotted lines for $\Gamma/M = 0.5$. Here $\Gamma/M \equiv \Gamma_B/M_B = \Gamma_C/M_C$.

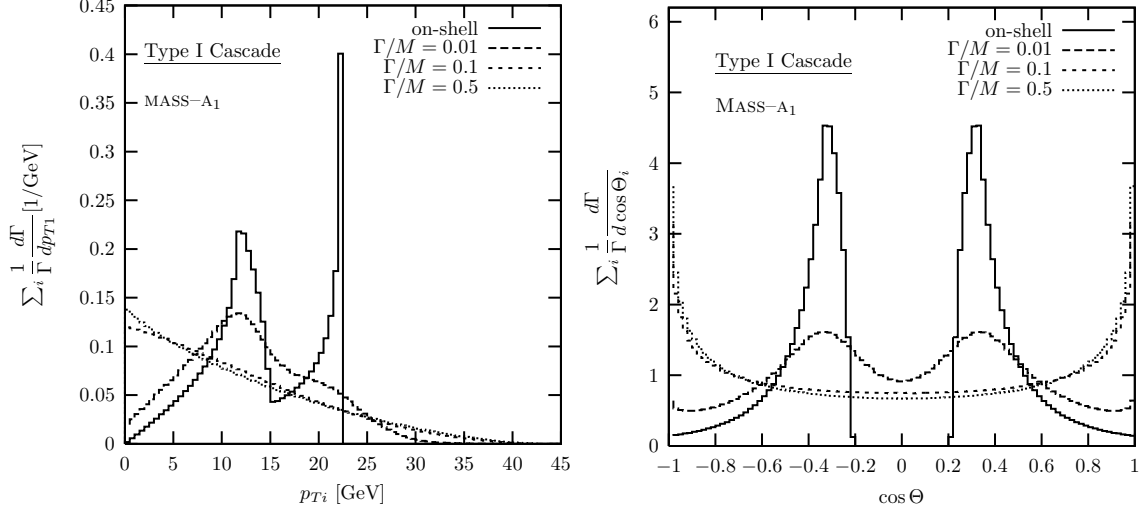


FIG. 15: The finite decay width effects on the summed distributions of p_{Ti} and $\cos \Theta_i$ in the MASS-A₁ case of the TYPE I cascade decay. As before, we take $\Gamma/M = 0, 0.01, 0.1, 0.5$.

destroys all of the sharp cusp structures into smooth peaks. In addition, the positions of the peaks are shifted significantly from the true cusp positions. For $\Gamma/M \gtrsim 0.1$ the summed p_{Ti} and $\cos \Theta_i$ distributions lose their functional characteristics completely, leaving very smooth and featureless distributions. In summary sizable widths like $\Gamma/M \gtrsim 0.01$ smash the cusps.

The fast-falling endpoints in the m , m_T , and p_{Ti} distributions are also smeared out

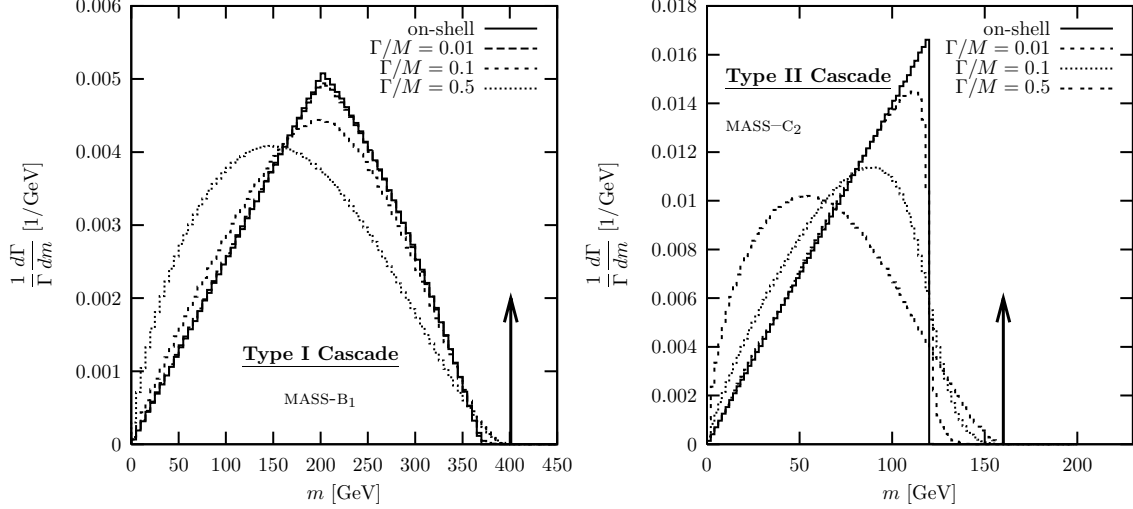


FIG. 16: Finite width effects on the normalized m distribution. We take the MASS-B₁ case for TYPE I decay, and MASS-C₂ for TYPE II decay. As before, we take $\Gamma/M = 0, 0.01, 0.1, 0.5$.

considerably. The degree of its shifting is large even for $\Gamma/M = 1\%$. One interesting observation is that two shifted endpoints of the m and m_T distributions are the same as $m_D - 2m_X$, denoted by vertical arrows. This new endpoint is from the kinematic configuration where two visible particles' momenta span all of the phase space determined by m_D and m_X . Even though we do not know the intermediate particle masses, the missing particle mass m_X can be read off. For this information, the m_T distribution is more advantageous than the m distribution, because of its fast falling shape.

In a realistic new physics process, however, this MASS-A₁ case does not allow even one percent of Γ/M . For example, the $Z^{(2)}$ decay in the minimal UED model has the decay widths of

$$\Gamma_D = \Gamma_{Z^{(2)}} \simeq 270 \text{ MeV}, \quad \Gamma_C = \Gamma_{L^{(2)}} \simeq 5 \text{ MeV}, \quad \Gamma_B = \Gamma_{L^{(1)}} \simeq 1 \text{ MeV}, \quad (32)$$

which leads to $\Gamma/M \sim 10^{-5}$. In summary, the extreme MASS-A₁ case has generically negligible width effects. The cusp and endpoint structures are reserved.

We consider more general mass parameters, MASS-B₁ for the TYPE I and MASS-C₂ for the TYPE II cascade decay. First we examine the finite width effects on the invariant mass distributions in Fig. 16. These cases show more stable cusp and endpoint structures from the finite width effects. For $\Gamma/M = 1\%$, the m distributions in both TYPE I and TYPE II decays do not change, keeping the same cusp and endpoint structures. For 10%

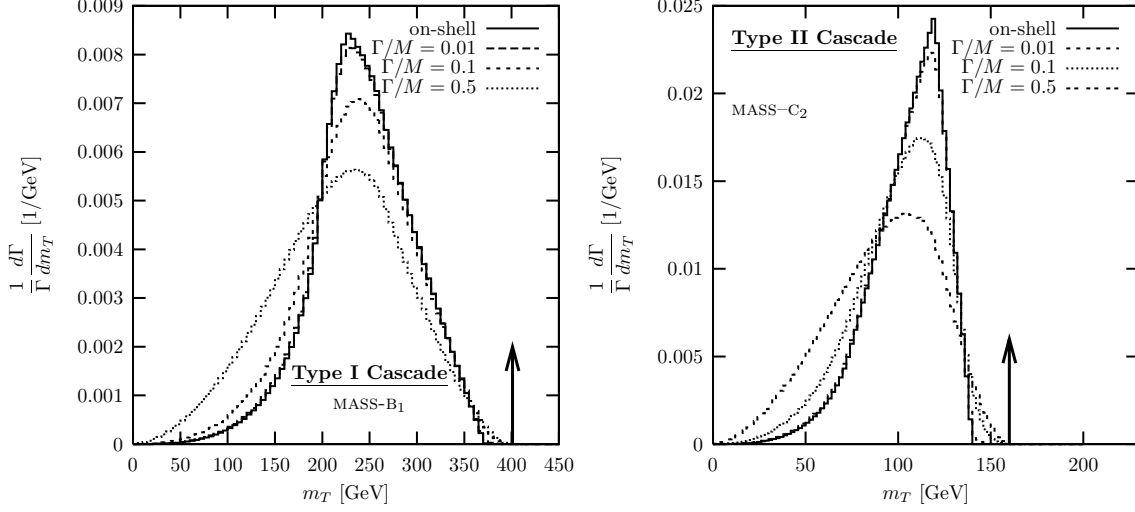


FIG. 17: The width effects on the normalized $d\Gamma/dm_T$ for the TYPE I MASS-B₁ and TYPE II MASS-C₂ cascade decays. As before, we take $\Gamma/M = 0, 0.01, 0.1, 0.5$.

of Γ/M , the m cusp of the TYPE I decay retains its position, though losing its sharpness. The m endpoints in both TYPE I and TYPE II decays are shifted into the new position $m_D - 2m_X$. If $\Gamma/M = 50\%$, the TYPE I decay does not retain the shape and position of the m cusp, and the TYPE II decay loses the right-angled triangle shape of the m distribution. Both cases have the same new endpoint at $m_D - 2m_X$, which is also valuable information for the missing particle mass measurement.

In Fig. 17, we show the width effects on the m_T distributions. The m_T cusp structures are more stable than the m cusps in both TYPE I and TYPE II decays. For $\Gamma/M = 1\%$, the changes in the distribution are unnoticeable. For $\Gamma/M \gtrsim 10\%$, we start to lose the sharpness of the cusps but still keep the positions for the cusp in both cases. If $\Gamma/M = 50\%$, the cusped peaks become dull further with relatively stable positions, and the m_T endpoints are shifted into $m_D - 2m_X$.

Figures 18 and 19 show the width effects on the summed distributions of p_{Ti} and $\cos \Theta_i$ respectively. Both distributions preserve the cusp structure for $\Gamma/M = 1\%$. If $\Gamma/M \gtrsim 10\%$, however, the finite width effects almost smear the cusp and endpoint structures.

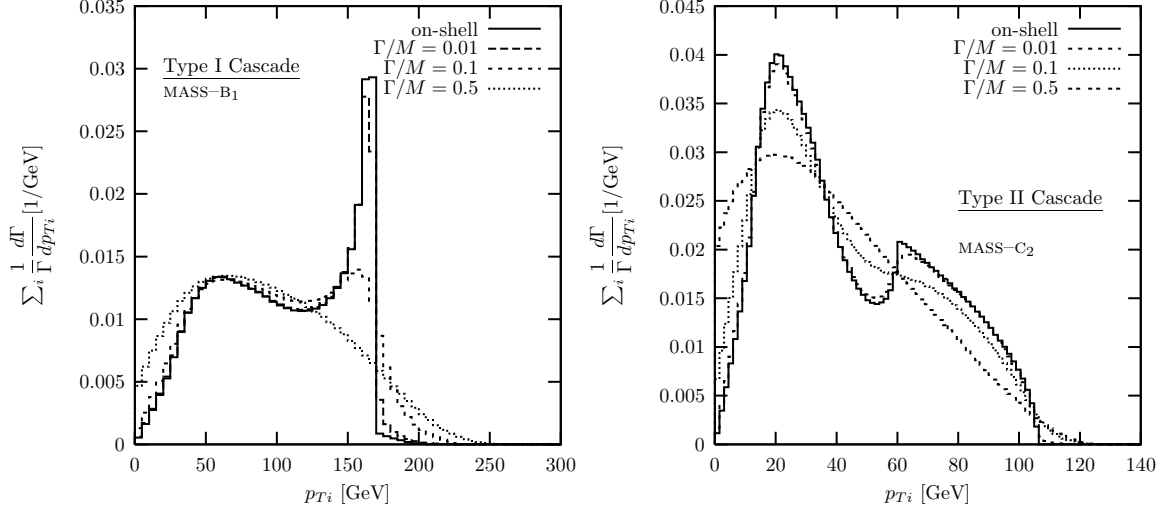


FIG. 18: The width effects on the summed distributions of p_{Ti} for $\Gamma/M = 0, 0.01, 0.1, 0.5$.

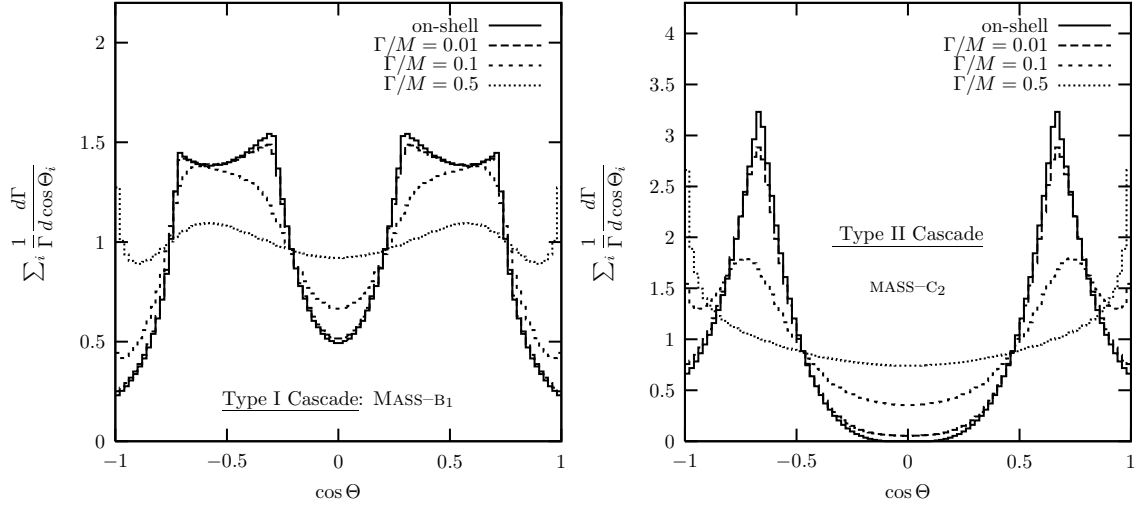


FIG. 19: The summed $\cos \Theta$ distributions for $\Gamma/M = 0, 0.01, 0.1, 0.5$.

B. Longitudinal boost effect

In hadronic collisions, the longitudinal motion of the particle D is not determined. This longitudinal ambiguity affects the kinematic variable $\cos \Theta$, which is defined in the D rest frame. In order to see the longitudinal boost effects, we convert the $\cos \Theta$ distribution in the D rest frame into the pp frame at the LHC, by convoluting with the parton distribution functions of a proton. In Fig. 20, we compare the summed distributions of $\cos \Theta_i$ in the D -rest frame (thin curves) with that in the pp lab frame at $\sqrt{s} = 14$ TeV (thick curves). For the parton distribution function, we have used CTEQ6 [28]. We take the MASS-A₁ for

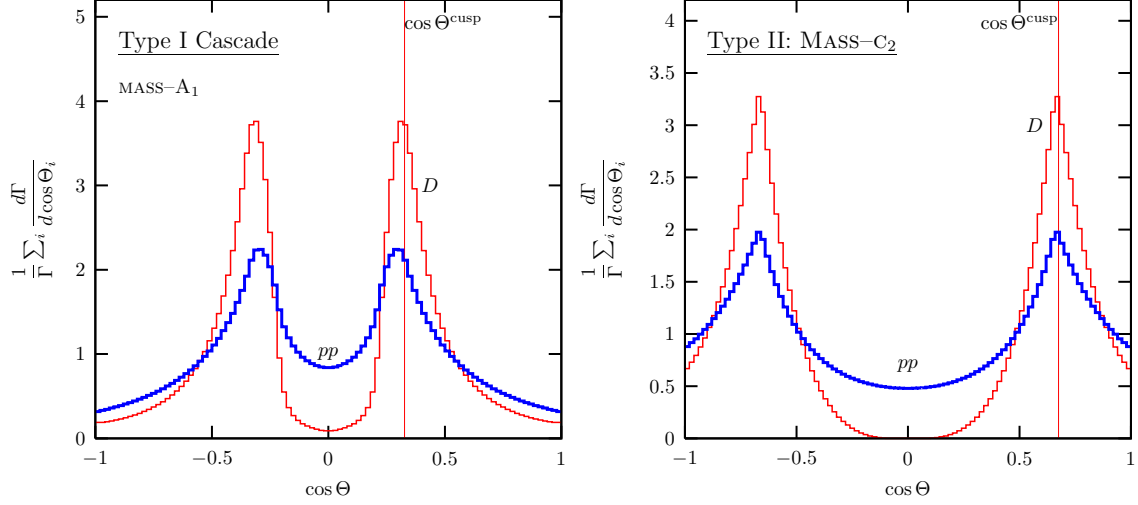


FIG. 20: Normalized differential decay rates versus $\cos \Theta$ in the D -rest frame (thin curves) and in the pp lab frame with $\sqrt{s} = 14$ TeV (thick curves).

TYPE I and the MASS-C₂ for TYPE II decay. For simplicity we assume that the heavy particle D is singly produced through the s -channel gluon fusion.

Unlike the finite width effects, the longitudinal boost effect does not completely smash the characteristic shape. The sharp cusp structures survive to some extent in both TYPE I and TYPE II cascade decays. The shift of the $\cos \Theta$ cusp position is minor. Moreover the overall functional shape remains the same even though the pp frame allows non-vanishing events around $\cos \Theta = 0$. The cusp in the $\cos \Theta$ distribution, though Lorentz non-invariant, is quite useful to draw mass information. Again we emphasize that the e^+e^- linear collider does not have this ambiguity.

C. ISR effects

The cusps and endpoints in the m_T and p_{Ti} distributions play a crucial role in the mass measurement of cascade, especially TYPE II, decays. The results are based on the assumption that the transverse momentum of the mother particle D is known event by event so that its rest frame along the transverse direction can be reconstructed. At a hadron collider, even though D is singly produced at the parton level, the gluon radiation from initial patrons, called the ISR, is inevitable because of strong QCD interaction: the mother particle D receives transverse kick and the ambiguity arises in its transverse motion [30].

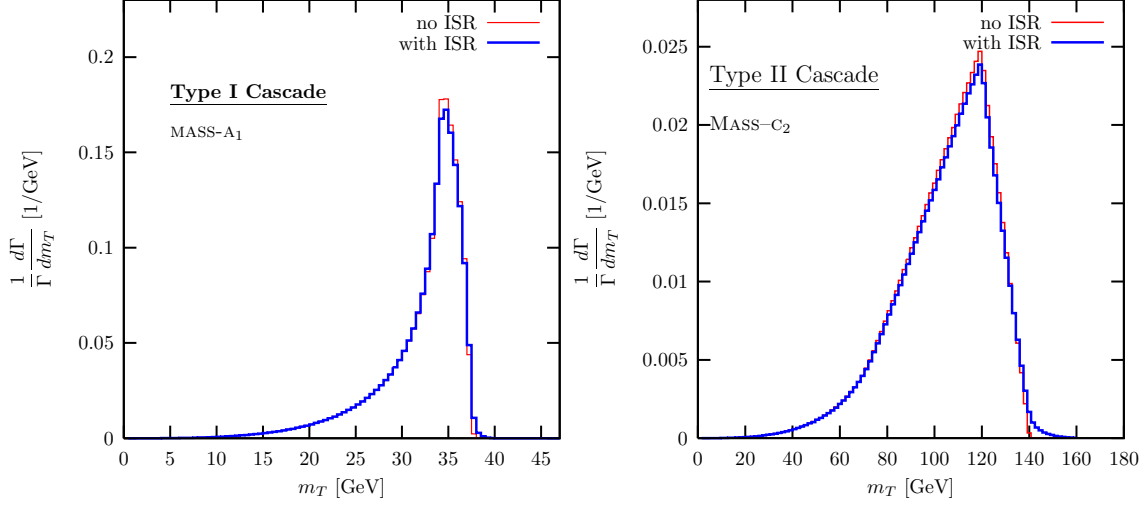


FIG. 21: The normalized transverse mass distributions with and without the ISR effects by the thin (red) line and the thick (blue) line, respectively. We take MASS-A₁ for the TYPE I cascade decay and MASS-C₂ for the TYPE II. Extra jets with $p_T > 50$ GeV are vetoed.

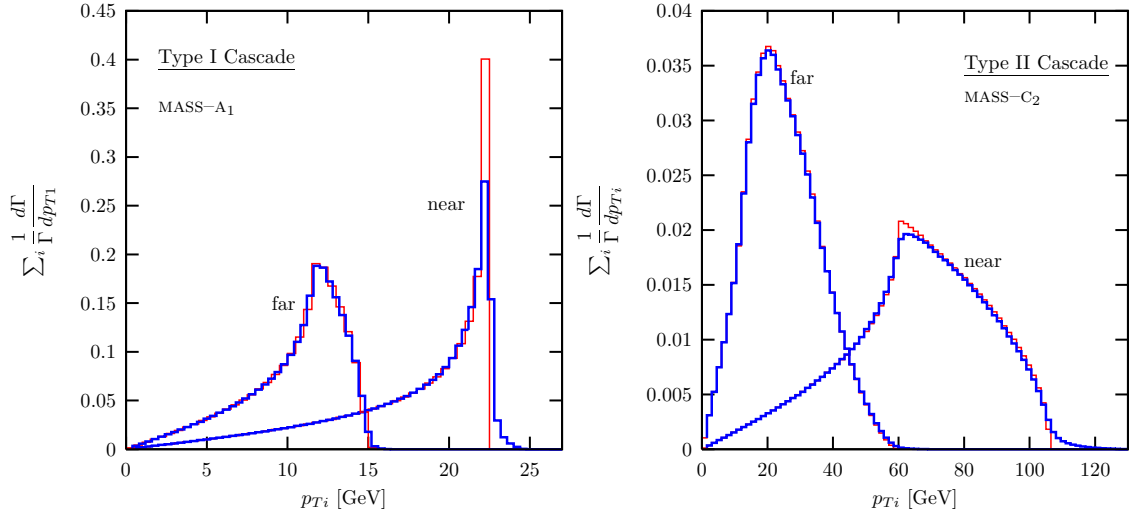


FIG. 22: The normalized p_{Tn} and p_{Tf} distributions with and without the ISR effects by the thin (red) line and the thick (blue) line, respectively. We take MASS-A₁ for the TYPE I cascade decay and MASS-C₂ for the TYPE II. Extra jets with $p_T > 50$ GeV are vetoed.

We examine the ISR effects on the cusp and endpoint structures in the m_T and p_{Ti} distributions. As in Ref. [17], we adopt the simplifying assumptions that D is produced by $q\bar{q}$ initial states, and decays through electroweak interactions so that final state radiation is neglected. We also veto hard ISR gluons if $p_T^{\text{jet}} > 50$ GeV. We use the parton shower Monte

Carlos in PYTHIA for the ISR [31].

Figure 21 compares the m_T distributions with and without ISR effects, denoted by the thin (red) line and the thick (blue) line, respectively. We take MASS-A₁ for TYPE I cascade decay, and MASS-C₂ for TYPE II decay. In both cases, the m_T cusps remain almost intact from the ISR effects. The sharpness and position keep those in the D rest frame. The endpoints get tailed, but not significantly. Almost linearly dropping behaviors for both cases are preserved until the vicinity of endpoints. The extrapolation of the distribution will help to find the endpoint without the ISR effects.

In Fig. 22, we show the normalized p_{Tn} and p_{Tf} distributions with and without the ISR effects by the thin (red) line and the thick (blue) line, respectively, in the same setup as in Fig. 21. In the TYPE I cascade decay, the far visible particle accommodates both the cusp and endpoint singularities in its transverse momentum distribution. The ISR effects do not affect them. The near visible particle in the TYPE I decay has only spiky and suddenly ending endpoint. The ISR smears this into the tailed one. Still the fast dropping behavior survives to some extent, which can be used to read the endpoint without ISR effects. In the TYPE II cascade decay, the near particle p_{Ti} distribution has the cusp and endpoint. The ISR effects do not change the cusp while smear the endpoint. The p_{Ti} distribution of the far visible particle, which has only the endpoint, is not affected.

In summary, the inclusion of ISR with veto on hard jets does not change the cusp structures while gets the endpoint tailed.

D. Spin-correlation effect

Our main results are based on the kinematics only, ignoring the spin-correlation in the full matrix elements. Since this paper is focused on the basic properties of the kinematic singular structures in the cascade decays, full analysis for each new physics process is beyond the scope of this paper. Nevertheless we expect that the algebraic singularity origin of the cusp and endpoint keeps them stable under the spin correlation effects [29].

In order to demonstrate this, we consider one example, the $Z^{(2)}$ decay in the the UED model:

$$\text{Cascade TYPE I:} \quad Z^{(2)} \rightarrow \ell + L^{(2)} \rightarrow \ell + B^{(1)} L^{(1)} \rightarrow \ell \ell B^{(1)} B^{(1)}. \quad (33)$$

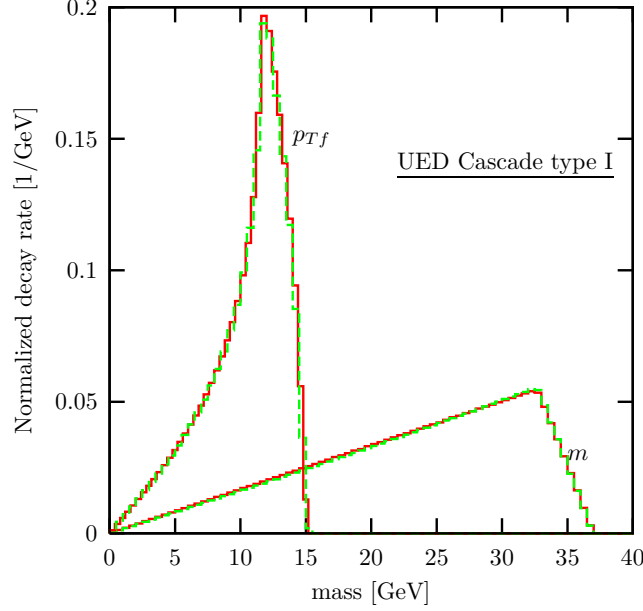


FIG. 23: The $d\Gamma/dm$ and $d\Gamma/dp_{T_i}$ for the process of $Z^{(2)} \rightarrow \ell + L^{(2)} \rightarrow \ell + B^{(1)}L^{(1)} \rightarrow \ell\ell B^{(1)}B^{(1)}$ with and without spin correlations.

In Fig. 23, we show their spin correlation effects. We find that the spin correlations do not change the m and p_{T_i} distributions. Two distributions with and without spin-correlation effects are almost identical.

We note that there are other uncertainties such as the SM background and experimental resolutions. The magnitudes of those effects depend on a specific process, which are beyond the scope of this paper. For a benchmark process of $pp \rightarrow Z' \rightarrow \tilde{\ell}^+\tilde{\ell}^- \rightarrow \ell^+\tilde{\chi}_1^0\ell^-\tilde{\chi}_1^0$ in a supersymmetry model with an extra $U(1)$ gauge field, we have considered all the realistic effects including the SM backgrounds and detector simulation in Ref. [16]. The total uncertainty in the mass measurement is about 10%. Most of the uncertainty is from huge SM $t\bar{t}$ backgrounds. Unless the observed decay products are jets, the experimental resolution does not affect the cusp and endpoint structures dominantly. The crucial role was done by best-fitting the m distribution based on its analytic functional form.

VI. SUMMARY AND CONCLUSIONS

We have studied the singularity structure, such as cusps and endpoints, in the kinematic distributions of three-step cascade decay of a new parity-even particle D and the determi-

	Antler	Cascade	
		TYPE I	TYPE II
m	yes	yes	no
m_T	no	yes	yes
p_T	no	no	no
p_{Tn}	yes	no	yes
p_{Tf}		yes	no
$\cos \Theta$	yes	yes	yes

TABLE III: The presence or absence of the cusp in the kinematic distributions of m , m_T , p_T , p_{Ti} , $\cos \Theta$ of the antler, TYPE I cascade, TYPE II cascade decays.

nation of the missing particle mass by using such singularities.

Two non-trivial decay topologies, called the TYPE I and TYPE II cascade decays, have been studied. In the TYPE I decay ($D \rightarrow a_1 C$, $C \rightarrow X_1 B$, $B \rightarrow a_2 X_2$), the distribution of the invariant mass m of two visible particles, a_1 and a_2 , develops a cusp. Full functional form of the m distribution for general mass parameters has been derived. If the mother particle D is produced at rest in the transverse direction, various longitudinal-boost invariant observables accommodate cusp structures. First the transverse mass m_T distribution has a cusp, which is complementary for the m cusp since the m_T cusp is sharp even when the m cusp is dull. Although the transverse momentum distribution of two visible particle system does not develop a visible cusp structure and a sharp endpoint, we note that the transverse momentum distribution of the far visible particle a_2 has a cusp, and that of the near visible particle a_1 has an endpoint of the shape of a steep cliff. We also study the summed distribution of $\cos \Theta_i$, which has two independent cusp structures.

In the TYPE II decay ($D \rightarrow X_1 C$, $C \rightarrow a_1 B$, $B \rightarrow a_2 X_2$), the kinematics of a_1 and a_2 is determined solely by the two-step cascade decay from the first intermediate particle C . The invariant mass distribution does not have a cusp structure. However, the kinematic distributions of the transverse motion carry the information from the whole three-step cascade decay. Both the m_T and $\sum_i p_{Ti}$ distributions have distinctive cusp structures. In the individual transverse momentum distribution, only the near visible particle has both a sharp cusp and a fast-falling endpoint. The $\cos \Theta$ distribution also shows a cusp as well. Includ-

ing the antler decay topology, we have summarized the existence of cusp in the kinematic distributions of m , m_T , p_T , p_{Ti} , and $\cos \Theta$ in Table III.

We have also considered the effects of the finite decay widths of intermediate particles, the longitudinal boost of the mother particle D , the ISR, and the spin correlation. The finite width effects are significant if the decay width is sizable like $\Gamma/M \gtrsim 10\%$: the sharp cusp gets smeared; the endpoint position gets shifted to $m_D - 2m_X$. The longitudinal motion of the mother particle D affects the distribution of $\cos \Theta$. At least for the sample mass parameters, however, the $\cos \Theta$ cusp remains sharp after convoluting with the parton distribution functions of a proton at the LHC. The ISR effects do not change the cusp structure much if we veto hard jets, but smear the endpoints. Spin correlation effects from full S -matrix elements turn out to be negligible in most cases, which is expected since the singularities are determined by the kinematic relations.

With the companion paper on the antler decay [17], our analysis presents the general properties and useful formulae of the kinematic cusps and endpoints for the decay topologies with two visible particles and two missing particles. By looking at the singularity structures of various kinematic distributions, the hidden nature of the missing particle can be probed effectively and elegantly. With the outstanding performance of the LHC and detectors, this is an exciting time for such investigation.

Acknowledgments

This work was supported in part by the U.S. Department of Energy under grant No. DE-FG02-12ER41832., and in part by PITT PACC. The work of JS was supported by WCU program through the NRF funded by the MEST (R31-2008-000-10057-0).

Appendix: Invariant mass distributions for the general Type I case

In this appendix, we present the invariant mass distribution in the general TYPE I cascade decays:

$$\begin{aligned}
 D(P) &\longrightarrow C + a_1(k_1), \\
 C &\longrightarrow B + X_1, \\
 B &\longrightarrow a_2(k_2) + X_2.
 \end{aligned}
 \tag{A.1}$$

As discussed in the main text, the TYPE II cascade decay is practically a three body decay in the view point of visible particles. This four-body decay has generally seven different mass parameters. We define the rapidities of six particles as

$$\begin{aligned}\cosh \xi_C &= \frac{m_D^2 + m_C^2 - m_{a_1}^2}{2m_D m_C}, & \cosh \xi_{a_1} &= \frac{m_D^2 + m_{a_1}^2 - m_C^2}{2m_D m_{a_1}}, \\ \cosh \xi_B &= \frac{m_C^2 + m_B^2 - m_{X_1}^2}{2m_C m_B}, & \cosh \xi_{X_1} &= \frac{m_C^2 + m_{X_1}^2 - m_B^2}{2m_C m_{X_1}}, \\ \cosh \xi_{a_2} &= \frac{m_B^2 + m_{a_2}^2 - m_{X_2}^2}{2m_B m_{a_2}}, & \cosh \xi_{X_2} &= \frac{m_B^2 + m_{X_2}^2 - m_{a_2}^2}{2m_B m_{X_2}}.\end{aligned}\tag{A.2}$$

A very useful kinematic variable is χ , the rapidity of the particle a_2 in the rest frame of a_1 :

$$\chi \equiv \cosh \xi_{a_2}^{(a_1)} = \frac{m^2 - m_{a_1}^2 - m_{a_2}^2}{2m_{a_1} m_{a_2}},\tag{A.3}$$

where the superscript (a_1) denotes that the rapidity is defined in the rest frame of a_1 .

The functional expression of $d\Gamma/dm$ is different according to the mass relations. The derivation of $d\Gamma/dm$ is similar to that presented in the appendix of Ref. [17]. For simple presentation, we introduce

$$\xi_{++} = \xi_B + \xi_{a_1} + \xi_{a_2} + \xi_C,\tag{A.4}$$

$$\xi_{+-} = |\xi_B + \xi_{a_1} - \xi_{a_2} - \xi_C|,\tag{A.5}$$

$$\xi_{-+} = |\xi_B - \xi_{a_1} + \xi_{a_2} + \xi_C|,\tag{A.6}$$

$$\xi_{--} = |\xi_B - \xi_{a_1} - \xi_{a_2} - \xi_C|.\tag{A.7}$$

We order ξ_{+-} , ξ_{-+} and ξ_{--} and name them $\xi_1 \leq \xi_2 \leq \xi_3$. Analytic functions forms of $d\Gamma/d\chi$ are then written as

- if $|\xi_B - \xi_{a_2} - \xi_C| \geq \xi_{a_1}$ or $\xi_B + \xi_{a_2} + \xi_C \leq \xi_{a_1}$,

$$\frac{d\Gamma}{d\chi} \propto \begin{cases} -\xi_1 + \cosh^{-1} \chi, & \text{if } \cosh \xi_1 \leq \chi \leq \cosh \xi_2, \\ \xi_2 - \xi_1, & \text{if } \cosh \xi_2 \leq \chi \leq \cosh \xi_3, \\ \xi_{++} - \cosh^{-1} \chi, & \text{if } \cosh \xi_3 \leq \chi \leq \cosh \xi_{++}, \\ 0, & \text{otherwise.} \end{cases}\tag{A.8}$$

- if $|\xi_B - \xi_{a_2} - \xi_C| < \xi_{a_1} < \xi_B + \xi_{a_2} + \xi_C$,

$$\frac{d\Gamma}{d\chi} \propto \begin{cases} 2 \cosh^{-1} \chi, & \text{if } 1 \leq \chi \leq \cosh \xi_1, \\ \xi_1 + \cosh^{-1} \chi, & \text{if } \cosh \xi_1 \leq \chi \leq \cosh \xi_2, \\ \xi_1 + \xi_2, & \text{if } \cosh \xi_2 \leq \chi \leq \cosh \xi_3, \\ \xi_{++} - \cosh^{-1} \chi, & \text{if } \cosh \xi_3 \leq \chi \leq \cosh \xi_{++}, \\ 0, & \text{otherwise.} \end{cases} \quad (\text{A.9})$$

The positions of the minimum, cusp, and maximum of the invariant mass distribution are

$$\begin{aligned} M_{\text{cas1}}^{\text{min}} &= \begin{cases} \sqrt{m_{a_1}^2 + m_{a_2}^2 + 2m_{a_1}m_{a_2} \cosh \xi_1}, & \text{for } \mathcal{R}_{1,\dots,6} \\ m_{a_1} + m_{a_2}, & \text{for } \mathcal{R}_{7,\dots,12} \end{cases} \quad (\text{A.10}) \\ M_{\text{cas1}}^{\text{cusp}} &= \sqrt{m_{a_1}^2 + m_{a_2}^2 + 2m_{a_1}m_{a_2} \cosh \xi_3}, \\ M_{\text{cas1}}^{\text{max}} &= \sqrt{m_{a_1}^2 + m_{a_2}^2 + 2m_{a_1}m_{a_2} \cosh \xi_{++}}. \end{aligned}$$

-
- [1] S. Perlmutter *et al.*, *Astrophys. J.* **517**, 565-586 (1999); A. G. Riess *et al.*, *Astron. J.* **116**, 1009-1038 (1998); A. G. Riess, R. P. Kirshner, B. P. Schmidt *et al.*, *Astron. J.* **117**, 707-724 (1999).
 - [2] E. J. Copeland, M. Sami, S. Tsujikawa, *Int. J. Mod. Phys. D* **15**, 1753-1936 (2006); L. M. Krauss, M. S. Turner, *Gen. Rel. Grav.* **27**, 1137-1144 (1995).
 - [3] G. Bertone, D. Hooper and J. Silk, *Phys. Rept.* **405**, 279 (2005).
 - [4] A. Djouadi, *Phys. Rept.* **459**, 1 (2008); G. Jungman, M. Kamionkowski and K. Griest, *Phys. Rept.* **267**, 195 (1996).
 - [5] G. Servant and T. M. P. Tait, *Nucl. Phys. B* **650**, 391 (2003); F. Burnell and G. D. Kribs, *Phys. Rev. D* **73**, 015001 (2006); K. Kong and K. T. Matchev, *JHEP* **0601**, 038 (2006).
 - [6] I. Low, *JHEP* **0410**, 067 (2004); A. Birkedal, A. Noble, M. Perelstein and A. Spray, *Phys. Rev. D* **74**, 035002 (2006); J. Hubisz and P. Meade, *Phys. Rev. D* **71**, 035016 (2005); A. Freitas, P. Schwaller and D. Wyler, *JHEP* **0912**, 027 (2009) [Erratum-ibid. **1102**, 032 (2011)].
 - [7] M. Burns, K. Kong, K. T. Matchev and M. Park, *JHEP* **0903**, 143 (2009).

- [8] I. Hinchliffe, F. E. Paige, M. D. Shapiro, J. Soderqvist and W. Yao, Phys. Rev. D **55**, 5520 (1997); H. Bachacou, I. Hinchliffe and F. E. Paige, Phys. Rev. D **62**, 015009 (2000); B. C. Allanach, C. G. Lester, M. A. Parker and B. R. Webber, JHEP **0009**, 004 (2000); B. K. Gjelsten, D. J. Miller and P. Osland, JHEP **0412**, 003 (2004); B. K. Gjelsten, D. J. Miller and P. Osland, JHEP **0506**, 015 (2005).
- [9] M. M. Nojiri, G. Polesello and D. R. Tovey, arXiv:hep-ph/0312317. K. Kawagoe, M. M. Nojiri and G. Polesello, Phys. Rev. D **71**, 035008 (2005).
- [10] H. C. Cheng, J. F. Gunion, Z. Han, G. Marandella and B. McElrath, JHEP **0712**, 076 (2007); M. M. Nojiri and M. Takeuchi, JHEP **0810**, 025 (2008); H. C. Cheng, D. Engelhardt, J. F. Gunion, Z. Han and B. McElrath, Phys. Rev. Lett. **100**, 252001 (2008).
- [11] C. G. Lester and D. J. Summers, Phys. Lett. B **463**, 99 (1999).
- [12] A. Barr, C. Lester and P. Stephens, J. Phys. G **29**, 2343 (2003); P. Meade and M. Reece, Phys. Rev. D **74**, 015010 (2006); S. Matsumoto, M. M. Nojiri and D. Nomura, Phys. Rev. D **75**, 055006 (2007); C. Lester and A. Barr, JHEP **0712**, 102 (2007).
- [13] W. S. Cho, K. Choi, Y. G. Kim and C. B. Park, Phys. Rev. Lett. **100**, 171801 (2008); B. Gripaios, JHEP **0802**, 053 (2008); A. J. Barr, B. Gripaios and C. G. Lester, JHEP **0802**, 014 (2008); W. S. Cho, K. Choi, Y. G. Kim and C. B. Park, JHEP **0802**, 035 (2008); M. M. Nojiri, Y. Shimizu, S. Okada and K. Kawagoe, JHEP **0806**, 035 (2008).
- [14] M. Serna, JHEP **0806**, 004 (2008); M. M. Nojiri, K. Sakurai, Y. Shimizu and M. Takeuchi, JHEP **0810**, 100 (2008).
- [15] H. -C. Cheng and Z. Han, JHEP **0812**, 063 (2008); A. J. Barr, B. Gripaios and C. G. Lester, JHEP **0911**, 096 (2009).
- [16] T. Han, I. W. Kim and J. Song, Phys. Lett. B **693**, 575 (2010).
- [17] T. Han, I. W. Kim and J. Song, arXiv:1206.5633 [hep-ph].
- [18] K. Agashe, D. Kim, M. Toharia and D. G. E. Walker, Phys. Rev. D **82**, 015007 (2010); W. S. Cho, D. Kim, K. T. Matchev and M. Park, arXiv:1206.1546 [hep-ph].
- [19] A. Datta, K. Kong and K. T. Matchev, Phys. Rev. D **72**, 096006 (2005) [Erratum-ibid. D **72**, 119901 (2005)]; H. C. Cheng, K. T. Matchev and M. Schmaltz, Phys. Rev. D **66**, 036005 (2002).
- [20] H. C. Cheng, K. T. Matchev and M. Schmaltz, Phys. Rev. D **66**, 036005 (2002).
- [21] T. Appelquist and H. U. Yee, Phys. Rev. D **67**, 055002 (2003).

- [22] T. G. Rizzo and J. D. Wells, Phys. Rev. D **61**, 016007 (1999); A. Strumia, Phys. Lett. B **466**, 107 (1999); C. D. Carone Phys. Rev. D **61**, 015008 (1999); I. Gogoladze and C. Macesanu Phys. Rev. D **74**, 093012 (2006).
- [23] P. Nath and M. Yamaguchi, Phys. Rev. D **60**, 116006 (1999); K. Agashe, N. G. Deshpande, and G. H. Wu Phys. Lett. B **511**, 85 (2001).
- [24] D. Chakraverty, K. Huiti, and A. Kundu, Phys. Lett. B **558**, 173 (2003); A. J. Buras, M. Spranger, and A. Weiler Nucl. Phys. B **660**, 225 (2003); A. J. Buras, A. Poschenrieder, M. Spranger, and A. Weiler Nucl. Phys. B **678**, 455 (2004); K. Agashe, N. G. Deshpande, and G. H. Wu, Phys. Lett. B **514**, 309 (2001).
- [25] B. Abbott *et al.*, D0 Collaboration, Phys. Rev. Lett. **83**, 4937 (1999).
- [26] S. Chang, K. Y. Lee and J. Song, Phys. Lett. B **707**, 144 (2012); S. Chang, K. Y. Lee and J. Song, Phys. Rev. D **85**, 055006 (2012); S. Chang, K. Y. Lee, S. Y. Shim and J. Song, arXiv:1207.6876 [hep-ph].
- [27] I. Hinchliffe, F. E. Paige, M. D. Shapiro, J. Soderqvist and W. Yao, Phys. Rev. D **55**, 5520 (1997); H. Bachacou, I. Hinchliffe and F. E. Paige, Phys. Rev. D **62**, 015009 (2000)
- [28] S. Kretzer, H. L. Lai, F. I. Olness, W. K. Tung, Phys. Rev. **D69**, 114005 (2004).
- [29] I. W. Kim, Phys. Rev. Lett. **104**, 081601 (2010).
- [30] Y.-K. Kim, U. Yang, CDF/PHY/TOP/CDFR/6804; J. M. Campbell, J. W. Huston and W. J. Stirling, Rept. Prog. Phys. **70**, 89 (2007) [hep-ph/0611148].
- [31] T. Sjostrand, S. Mrenna and P. Z. Skands, JHEP **0605**, 026 (2006) [hep-ph/0603175].